

Article

GEE-Based Ecological Environment Variation Analysis under Human Projects in Typical China Loess Plateau Region

Jingya Tang ^{1,2} , Lichun Sui ^{1,*}, Ting Ma ^{3,4}, Yang Dan ^{3,4}, Qian Yang ^{3,4}, Ruofan Zhao ⁵ and Xinhuan Qiang ¹

¹ School of Geological Engineering and Geomatics, Chang'an University, Xi'an 710064, China; 2019026003@chd.edu.cn (J.T.)

² Institute of Geography and Geoecology (IFGG), Karlsruhe Institute of Technology (KIT), 76131 Karlsruhe, Germany

³ College of Geomatics, Xi'an University of Science and Technology, Xi'an 710021, China

⁴ Key Laboratory of Coal Resources Exploration and Comprehensive Utilization, Ministry of Natural Resources, Xi'an 710054, China

⁵ Institute of Surveying and Mapping, Xi'an 710054, China

* Correspondence: sui1011@chd.edu.cn

Abstract: The China Loess Plateau (CLP) is a unique geomorphological unit with abundant coal resources but a fragile ecological environment. Since the implementation of the Western Development plan in 2000, the Grain for Green Project (GGP), coal mining, and urbanization have been extensively promoted by the government in the CLP. However, research on the influence of these human projects on the ecological environment (EE) is still lacking. In this study, we investigated the spatial-temporal variation of EE in a typical CLP region using a Remote Sensing Ecological Index (RSEI) based on the Google Earth Engine (GEE). We obtained a long RSEI time series from 2002–2022, and used trend analysis and rescaled range analysis to predict changing trends in EE. Finally, we used Geodetector to verify the influence of three human projects (GGP, coal mining, and urbanization). Our results show that GGP was the major driving factor of ecological changes in the typical CLP region, while coal mining and urbanization had significant local effects on EE. Our research provides valuable support for ecological protection and sustainable social development in the relatively underdeveloped region of northwest China.



Citation: Tang, J.; Sui, L.; Ma, T.; Dan, Y.; Yang, Q.; Zhao, R.; Qiang, X. GEE-Based Ecological Environment Variation Analysis under Human Projects in Typical China Loess Plateau Region. *Appl. Sci.* **2023**, *13*, 4663. <https://doi.org/10.3390/app13084663>

Academic Editor: Tiago Miranda

Received: 23 March 2023

Revised: 2 April 2023

Accepted: 4 April 2023

Published: 7 April 2023



Copyright: © 2023 by the authors. Licensee MDPI, Basel, Switzerland. This article is an open access article distributed under the terms and conditions of the Creative Commons Attribution (CC BY) license (<https://creativecommons.org/licenses/by/4.0/>).

Keywords: remote sensing ecological index; human projects; grain for green project; china loess plateau; Google Earth Engine; geodetector

1. Introduction

The China Loess Plateau (CLP) has been a pivotal region for the Chinese government in implementing strategies for environmental protection and sustainable development [1–4]. It spans over 640,000 km² and has a population of nearly 100 million. The surface of CLP is characterized by thick loess, complex geomorphology, aridity, and low rainfall, resulting in a fragile natural ecological environment (EE). Moreover, its urbanization process lags behind the east and central regions of China, and its land resources are relatively poor and unevenly distributed, despite its abundant underground coal and other mineral resources.

Since the beginning of the 21st century, the CLP has been a primary region for the implementation of China Western Development [5,6]. The region is characterized by mountains, plateaus, hills, gullies, and river valley plains. China Western Development was initiated by the Chinese government in 2000 to promote sustainable and balanced economic and social development. Its major programs include the Grain for Green Project (GGP) [7–10], coal mining [11], and urbanization [2,12,13], among others.

The GGP includes two aspects: Firstly, planting trees and forests instead of cultivating sloped ground in the loess hilly-gully regions, and secondly, hill-closing and afforestation of mountainous areas to restore forest vegetation. Since 2002, CLP has invested more

than 50 billion RMB in the GGP and reforested an area of 52,000 km², with one-third of the reforestation on arable land and the rest on barren hills and wastelands, as well as hill-closing and afforestation [14]. The growth rate of vegetation cover in CLP from 2000 to the present is much higher than the national average, resulting in significantly less sediment entering the Yellow River and reduced soil erosion, making CLP a leader in China's greening efforts. The utilization of coal resources is the pillar industry of economic development in the CLP. Since 2000, several coal production bases have been built in the region, and annual coal production now exceeds 2 billion tons, accounting for about 1/4 of global coal production, making CLP the major coal production base in China and the world [15]. The rapid development of four provincial capitals in the CLP's river valley plain has been supported by the Chinese government for the past 20 years, and a large number of rural and suburban areas have been transformed into urban areas, significantly increasing the region's development. After nearly three decades of resource development and EE construction, the CLP has become a key center for China's chemical and energy industry, as well as an ecological barrier for the entire northern region.

Due to the complex geomorphology and frequent human projects in CLP, it is currently poorly understood how the EE of CLP has changed over the last 20 years. GGP promotes the growth of vegetation cover and EE improvement in CLP, while coal mining damages the overlying strata, resulting in surface subsidence, collapse, and cracks, which cause EE deterioration [16]. Urbanization has caused arable or forest land to be turned into building land, resulting in serious ecological impacts [17,18]. Due to the significant temporal and spatial divergence of these three human projects in the last 20 years, the EE characteristics of CLP have become complex and unknown. Previous studies on the EE of CLP have mainly focused on the impacts of geographical and meteorological factors on the EE of a certain region, while scientific and quantitative studies on the impact of human projects on the EE of CLP are still lacking [19,20].

Remote sensing provides new tools for evaluating EE, especially those of ecosystems that include mining areas, forests, grasslands, and urban areas [21–25]. In the early stages of EE modeling, only single indicators were used [26–28]. However, due to the complexity of EE, it is insufficient to describe them using only one index. To overcome this, Xu et al. extracted indicators of greenness, heat, dryness, and wetness, and constructed a Remote Sensing Ecological Index (RSEI) based on Principal Component Analysis (PCA) [29]. This model has been successfully applied to different ecological scenarios [30–33]. However, EE faces challenges due to the large data size and difficulty in processing. The Google Earth Engine (GEE) can process large amounts of geospatial data and is a useful tool for large-scale and long-term ecological evaluation [34,35].

Currently, research on the EE evaluation of CLP remains insufficient. For example, Hou et al. evaluated the EE of the coal mining area in Datong, Shanxi Province, China by integrating RS, GIS, and field survey methods [36]. Zhou et al. analyzed land-use and land-cover changes caused by the GGP in China's CLP [37,38]. Xiang et al. constructed an urbanization index using nighttime lighting data and examined the spatial and temporal evolution of urbanization in CLP [39]. Previous studies on EE in the CLP have primarily focused on analyzing the impact of individual factors on a specific region or the entire region. However, there has been limited research examining the impact of multiple factors on EE. Given the diverse landforms of the Loess Plateau, which includes numerous mining and urban regions, it is important to select representative areas for detailed analysis, especially in light of the GGP.

Due to the variability of CLP's geomorphology, the ecological impact of GGP varies significantly in different geomorphological units. For example, hilly and gully regions are generally where GGP is implemented, while river valley plain regions are mostly urbanization expansion regions, and coal mining affects the variation of EE in nearby regions. In this study, we comprehensively analyzed the temporal and spatial characteristics of ecological environment (EE) changes in typical regions of the China Loess Plateau (CLP) from 2002 to 2022. We used MODIS time-series images and the Remote Sensing Ecological Index

(RSEI) constructed through principal component analysis (PCA) to analyze the temporal characteristics of EE changes. Additionally, we evaluated the spatial characteristics of EE variations in the entire study area and investigated the impacts of coal mining and urbanization on EE in sample regions such as the Dafosi mine and the Guanzhong Plain urban agglomeration in CLP. Based on the long RSEI time series, we predicted the EE evolution trend. Finally, to verify the conclusions made in this paper, we introduced Geodetector to perform an attribution analysis of the factors resulting in EE evolution in CLP.

In summary, the authors studied the temporal–spatial variation of EE in the study area since 2002 under the influence of GGP, coal mining, and urbanization. The results support the achievement of green and sustainable development in the relatively underdeveloped region in northwestern China.

2. Study Area and Data

2.1. Study Area

The CLP ($33^{\circ}43'7''$ – $41^{\circ}16'7''$ N and $100^{\circ}54'7''$ – $114^{\circ}33'7''$ E) is situated in north–central China and covers an area of nearly 640,000 km² [40]. The region is characterized by four main types of landforms: Mountain regions, loess tableland regions, loess hilly-gully regions, and river valley regions [41]. In 1999, the Chinese government implemented the GGP to improve the EE of CLP, with Shaanxi province serving as the pilot region [42].

The study area ($33^{\circ}7'$ – $36^{\circ}4'$ N and $105^{\circ}7'$ – $110^{\circ}6'$ E) is located in a typical CLP region in Shaanxi province, comprising the Huanglong coal base, the Xi'an-centered Guanzhong plain urban agglomeration, and the GGP (including GGP regions and hill-closing and afforestation regions), as shown in Figure 1 [43]. The loess tableland and loess hilly-gully regions are mostly located north of the Weihe River, while the river valley plains and mountainous regions are mostly situated south of the Weihe River. The Huanglong coal base is located north of the Weihe River [44], while the Guanzhong plain urban agglomeration is located south of the Weihe River. Figure 1 also illustrates the distribution of landforms in the study area.

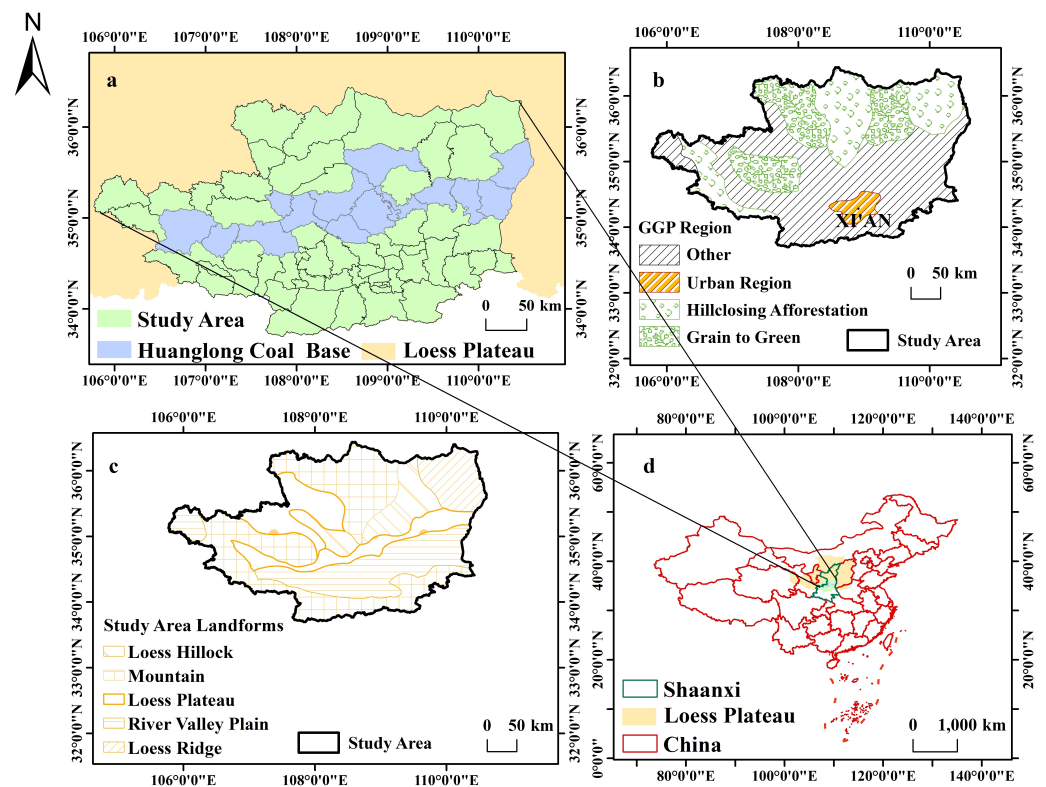


Figure 1. Study area overview: (a) Study area; (b) distribution of coal mining, GGP, urbanization regions in the study area; (c) landform classification of the study area; (d) location of the study area in China.

Due to the abundant coal resources in CLP, coal mining has a significant impact on the EE. The Huanglong coal base is located in central Shaanxi province and is one of the 14 large coal bases that China is focused on developing. The landform of the Huanglong coal base is complex, with elevations ranging from about 400–1850 m. The main landforms in the area are loess hilly-gully. However, the resistance to deformation of the loess layer is very small, and coal mining can lead to ground deformation and collapse, as shown in Figure 2. Large-scale mining operations in the Huanglong coal base began in the early 1980s, and as a result of mining and other human projects, the EE became poor in the early 21st century.

The China Western Development strategy, which began in 2000, coincided with the implementation of the GGP and has resulted in the rapid expansion of the Guanzhong plain urban agglomeration. The extensive urban construction has had a negative impact on the EE in the surrounding area. The urban agglomeration is centered in Xi'an, Shaanxi Province, which is situated in the river valley plain region.

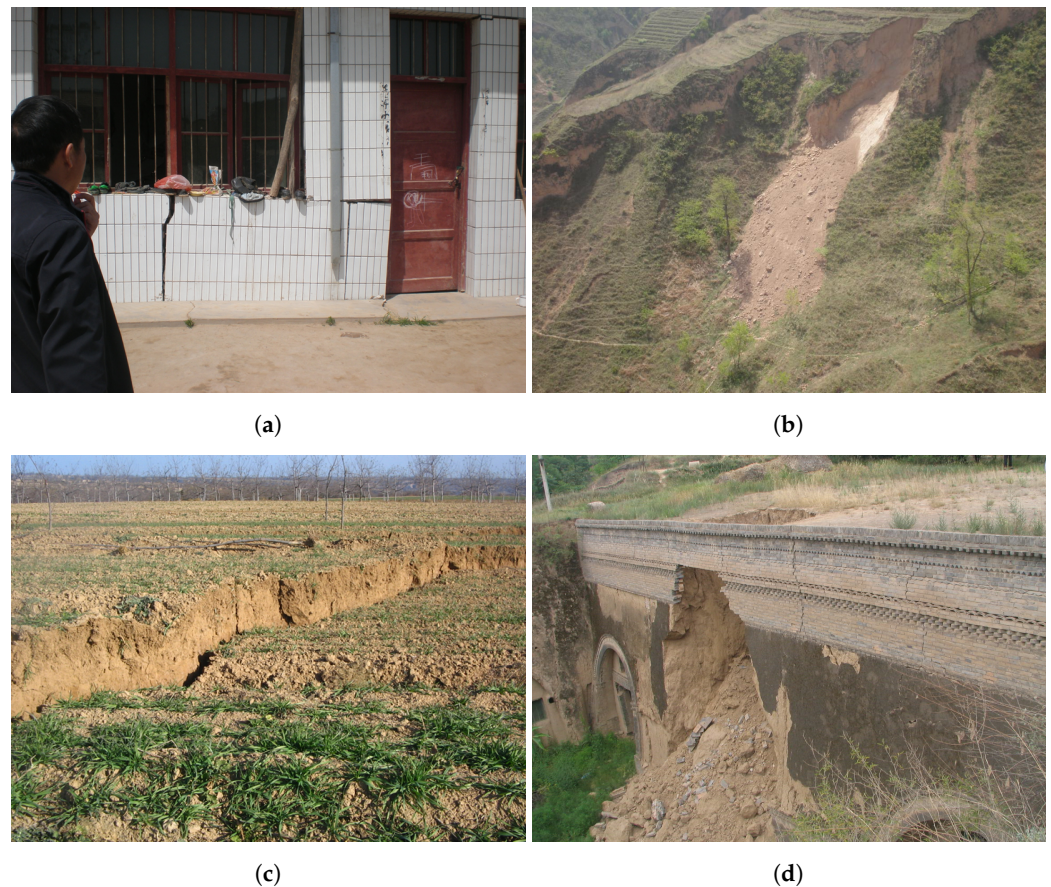


Figure 2. Deformation and subsidence cause by underground coal mining. (a) Building deformation; (b) landslide; (c) ground cracks; (d) ground collapse.

2.2. Data and Preprocessing

The remote sensing data used in this study were obtained from the Google Earth Engine (GEE) (<https://earthengine.google.com/>, accessed on 22 March 2023), with a collection period ranging from 2002 to 2022. The MOD09A1 (MOD09A1.006 Terra Surface Reflectance 8-Day Global 500 m) and MOD11A1 (MOD11A1.061 Terra Land Surface Temperature and Emissivity Daily Global 1 km) products available in GEE were used to calculate the greenness (NDVI), wetness (WET), and dryness (NDBSI) indices based on the MOD09A1 products, and the heat (LST) index based on the MOD11A1 products. Please refer to Table 1 for more details on the datasets used in this study.

The data on China’s administrative division boundaries were obtained from the National Geomatics Center of China (<http://www.ngcc.cn/ngcc/>, accessed on 22 March 2023). The GGP and urban planning data were obtained from the National Science and Technology Infrastructure (<http://www.nesdc.org.cn/>, accessed on 22 March 2023). The landform data for the study area were obtained from the National Earth System Science Data Center (<http://www.geodata.cn/>, accessed on 22 March 2023). The precipitation and temperature data for the study area were obtained from the China Meteorological Data Service Centre (<http://data.cma.cn/>, accessed on 22 March 2023).

The annual mining area data of the Dafosi coal mine were obtained through the comparison of working-face images and field measurements. Land-use/land-cover (LULC) data from 2000 to 2021 for the study area were obtained from the China Land Cover Dataset (CLCD) based on Landsat data from the GEE. LULC data for 2022 were obtained through the interpretation of Landsat 8 OLI_TRIS 30 m remote sensing images from the United States Geological Survey (<https://earthexplorer.usgs.gov/>, accessed on 22 March 2023). The remote sensing images were analyzed, corrected, fused, and mosaicked using ArcGIS 10.6 and ENVI 5.3, and the land use types were classified using a combination of supervised classification and visual interpretation. Per capita GDP, the area of GGP, and coal production data were obtained from the Statistical Communiqué of the People’s Republic of China on the national economic and social development from 2000 to 2021.

Table 1. GEE data description.

Indicator	Product	Spatial Resolution	Temporal Resolution	Number of Scenes
NDVI WET NDBSI	MOD09A1	500	8-Days	16
LST	MOD11A1	1000	1-Days	122

3. Methods

3.1. RSEI

Using MODIS remote sensing data to describe the EE level [22], the RSEI takes a value ranging from 0 to 1, where a low value indicates a poor ecological condition, a high value represents a good ecological condition, and a value of 1 signifies a perfect ecological condition. MODIS remote sensing data collected between June and October in 2002, 2007, 2012, 2017, and 2022 were used to calculate the RSEI. The four indicators utilized in the RSEI are greenness (NDVI for vegetation), wetness (WET for soil wetness), heat (LST for temperature), and dryness (NDBSI for floor area). By coupling and integrating the four indicators and using the PCA, the weights of each indicator are automatically determined, avoiding any interference from human-determined weights. Then, the first principal component (PC1) is obtained, and the RSEI assessment model is constructed. The RSEI is expressed as:

$$RSEI = f(NDVI, Wet, LST, NDBSI) \tag{1}$$

- Greenness can be calculated by:

$$NDVI = (\rho_{NIR} - \rho_{red}) / (\rho_{NIR} + \rho_{red}), \tag{2}$$

where *NIR* and *red* are the near-infrared (NIR1) and red bands of the MODIS 8-day reflectance image (MOD09A1), respectively.

- Wetness is calculated using the following equation [45]:

$$Wet = 0.1147B1 + 0.2489B2 + 0.2408B3 + 0.3132B4 - 0.3122B5 - 0.6416B6 - 0.5087B7 \tag{3}$$

Here, B1 to B7 represent bands 1 to 7, namely, red, NIR1, blue, green, NIR2, shortwave infrared 1 (SWIR1), and SWIR2 bands of the MODIS images, respectively.

- Heat is expressed as:

$$LST = 0.02 \times DN - 273.15 \tag{4}$$

where DN represents the grayscale value of the surface temperature.

- Dryness is expressed as follows:

$$NDBSI = \frac{IBI + SI}{2} \tag{5}$$

The Building Index (IBI) and Bare Soil Index (SI) can be calculated as follows:

$$SI = \frac{(\rho_{swir1} + \rho_{red}) - (\rho_{nir} + \rho_{blue})}{(\rho_{swir1} + \rho_{red}) + (\rho_{nir} + \rho_{blue})} \tag{6}$$

$$IBI = \frac{\frac{2\rho_{swir1}}{\rho_{swir1} + \rho_{nir}} - \left[\frac{\rho_{nir}}{\rho_{nir} + \rho_{red}} + \frac{\rho_{green}}{\rho_{green} + \rho_{swir1}} \right]}{\frac{2\rho_{swir1}}{\rho_{swir1} + \rho_{nir}} + \left[\frac{\rho_{nir}}{\rho_{nir} + \rho_{red}} + \frac{\rho_{green}}{\rho_{green} + \rho_{swir1}} \right]} \tag{7}$$

where ρ_{blue} , ρ_{green} , ρ_{red} , ρ_{NIR} , ρ_{swir1} represent the reflectance in the blue, green, red, the near-infrared and short-infrared bands1, respectively.

- PCA: Since the four indicators have non-uniform magnitudes, calculating the PCA directly would result in unbalanced weights for each indicator. Therefore, before conducting PCA, these indicators should be normalized first, and their magnitudes should be unified to the range [0, 1] using the following equation:

$$NI_i = (I_i - I_{min}) / (I_{max} - I_{min}) \tag{8}$$

where NI_i is the normalized indicator value, I_i is the indicator value in quadrant i , I_{max} is the maximum indicator value, and I_{min} is the minimum indicator value.

After normalization, PC1 can be calculated using the four indicators. In order to ensure that a larger PC1 value represents a better condition, PC1 is subtracted by 1 to obtain the initial ecological indicator $RSEI_0$. The calculation is as follows:

$$RSEI_0 = 1 - \{PC1[f(NDVI, WET, LST, NDBSI)]\} \tag{9}$$

$$RSEI = (RSEI_0 - RESEI_{0min}) / (RSEI_{0max} - RESEI_{0min}) \tag{10}$$

Because PC1 usually explains more than 80% of the total variation in the dataset, it is used to calculate the RSEI, then the bias due to subjective weighting during the calculation is avoided. The RSEI calculation results for each indicator for 2002, 2007, 2012, 2017, and 2022 are shown in Table 2.

The ecological quality of the study area is classified into five levels based on the normalized RSEI values: Level 1 (0–0.2) representing poor ecological quality, level 2 (0.2–0.4) representing fair ecological quality, level 3 (0.4–0.6) representing moderate ecological quality, level 4 (0.6–0.8) representing good ecological quality, and level 5 (0.8–1) representing excellent ecological quality. Table 3 presents the ecological quality classes and the corresponding area changes in the study area for different years.

Table 2. Calculation results of the four indicators of RSEI in the study area.

Year	Indicator	PC1	PC2	PC3	PC4
2002	NDVI	0.562	0.459	−0.541	−0.425
	WET	0.186	−0.697	0.136	−0.679
	NDBSI	−0.445	0.528	0.438	−0.576
	LST	0.672	0.159	0.705	0.163
2007	NDVI	0.59	0.379	−0.562	−0.439
	WET	0.169	−0.707	0.211	−0.653
	NDBSI	0.564	−0.501	−0.226	0.616
	LST	−0.552	−0.324	−0.767	−0.04
2012	NDVI	0.549	0.387	−0.559	−0.484
	WET	0.143	−0.739	0.177	−0.632
	NDBSI	0.514	−0.498	−0.357	0.598
	LST	−0.642	−0.234	−0.726	−0.0766
2017	NDVI	0.584	0.397	−0.551	−0.444
	WET	0.195	−0.785	0.107	−0.578
	NDBSI	−0.483	0.428	0.346	−0.68
	LST	0.622	0.206	0.751	0.069
2022	NDVI	0.562	0.401	−0.565	−0.452
	WET	0.216	−0.776	0.127	−0.578
	NDBSI	−0.423	0.446	0.426	−0.663
	LST	0.677	0.195	0.695	0.145

Table 3. The changes in ecological quality levels and their corresponding areas in the study area over different years.

RSEI Level		Poor ([0,0.2])	Fair ([0.2,0.4])	Moderate ([0.4,0.6])	Good ([0.6,0.8])	Excellent ([0.8,1.0])
2002 Year	Area (km ²)	9196.26	25,544.56	18,963.00	13,027.19	15,637.21
	Pct. (%)	11.17	31.01	23.02	15.81	18.99
2007 Year	Area (km ²)	6213.92	19,830.64	23,569.50	15,811.50	16,939.65
	Pct. (%)	7.54	24.08	28.62	19.20	20.57
2012 Year	Area (km ²)	6519.46	18,218.97	22,170.11	16,813.65	18,643.03
	Pct. (%)	7.92	22.12	26.92	20.41	22.63
2017 Year	Area (km ²)	7696.82	19,154.39	18,294.59	16,262.18	20,957.22
	Pct. (%)	9.34	23.26	22.21	19.74	25.44
2022 Year	Area (km ²)	6316.27	16,977.38	20,176.02	17,115.69	21,779.85
	Pct. (%)	7.67	20.61	24.50	20.78	26.44

3.2. Change Vector Analysis (CVA)

The method assumes that the images at two different time phases can be represented as vectors *R* and *T*, respectively. It quantifies the degree of change by calculating the difference vector between *R* and *T*. A threshold value is then used to filter out regions where changes occur between the two phases [22].

$$R = \begin{bmatrix} r_1 \\ r_2 \\ \vdots \\ r_n \end{bmatrix}, T = \begin{bmatrix} t_1 \\ t_2 \\ \vdots \\ t_n \end{bmatrix} \tag{11}$$

where n denotes the indicator number or the RSEI levels. The transformation vector is determined by the following equation.

$$\Delta V = \mathbf{R} - \mathbf{T} = \begin{bmatrix} r_1 - t_1 \\ r_2 - t_2 \\ \vdots \\ r_n - t_n \end{bmatrix} \tag{12}$$

The magnitude of the change $|\Delta V|$ can be calculated using Equation (13). The greater the $|\Delta V|$, the greater the likelihood that the RSEI in the region will change.

$$\|\Delta V\| = \left[(r_1 - t_1)^2 + (r_2 - t_2)^2 + \dots + (r_n - t_n)^2 \right]^{\frac{1}{2}} \tag{13}$$

To identify changes in the metrics, a multi-threshold approach is employed:

$$CV_j(\mathbf{R}, \mathbf{T}) = \begin{cases} \text{change, if } \|\Delta V_j\| \geq \overline{\Delta V_j} + a_j \sigma_j \\ \text{no - change, } \|\Delta V_j\| < \overline{\Delta V_j} + a_j \sigma_j \end{cases} \tag{14}$$

In this equation, $\overline{\Delta V_j}$ represents the average of the transformed vector for the j th term, σ_j is the standard deviation of ΔV_j , and a_j is an adjustable coefficient with a value range of [0.06, 0.18].

3.3. Spatial Auto-Correlation

The Global Moran's index is used to analyze the global spatial correlation of EE, while the local Moran's index is employed to analyze the local spatial aggregation characteristic. These indices can be calculated using the following equations [46–48]:

$$\begin{aligned} \text{Global Moran's Index} &= \frac{n}{S_0} \frac{\sum_{i=1}^n \sum_{j=1}^m w_{ij} z_i z_j}{\sum_{i=1}^n z_i^2} \\ \text{Local Moran's Index} &= \frac{nz_i \sum_{j=1}^m w_{ij} z_j}{\sum_{i=1}^n z_i^2} \end{aligned} \tag{15}$$

The deviation of the RSEI value at spatial cell i from its mean value, denoted as $z_i = (x_i - \bar{X})$, is used in the formula, where \bar{X} is the mean value of the RSEI. The spatial weight matrix is represented by w_{ij} , n is the total number of elements, and S_0 represents the aggregation of all spatial weights.

$$S_0 = \sum_{i=0}^n \sum_{j=0}^m w_{ij} \tag{16}$$

The Moran index I ranges from -1 to 1 , and a higher absolute value indicates a stronger spatial autocorrelation. A positive I value implies a positive correlation, while a negative value implies a negative correlation. An I value of 0 indicates no spatial correlation. The local Moran index, calculated using the Local Indicators of Spatial Association (LISA), is used to assess the degree of local spatial correlation. LISA plots are categorized into five groups: Insignificant, high-high (HH), low-low (LL), low-high (LH), and high-low (HL).

3.4. RSEI Transfer Matrix

In order to accurately depict the variation of RSEI levels over time, area, and location, a transfer matrix is utilized to describe the changes in the amount of EE on a temporal scale

and the changes in location on a spatial scale [49]. The RSEI transfer matrix is constructed by overlaying RSEI values from different time periods, and can be expressed as:

$$S = \begin{pmatrix} S_{11} & S_{12} & \cdots & S_{1j} \\ S_{21} & S_{22} & \cdots & S_{2j} \\ \cdots & \cdots & \cdots & \cdots \\ S_{i1} & S_{i2} & \cdots & S_{ij} \end{pmatrix} \tag{17}$$

The RSEI levels at the beginning and end of the study are denoted by i and j ($i = 1, 2, \dots, n; j = 1, 2, \dots, n$), respectively. The area where the i th RSEI level at the beginning of the study is transferred to the j th RSEI level at the end of the study period is represented by S_{ij} .

3.5. Geodetector-Based Driving Force Analysis

The present study employs the Geodetector to undertake the analysis of driving forces and quantitative attribution of EE, where the factor detector is utilized. Within the factor detector, the q value is introduced as a metric to indicate the explanatory ability of different factors on the degree of spatial differentiation of the dependent variable. The q value is bound within the range $[0, 1]$, where a larger value indicates a more influential factor.

$$q = 1 - \frac{SSW}{SST} = 1 - \frac{\sum_{i=1}^k N_i \sigma_i^2}{N \sigma^2} \tag{18}$$

where SSW refers to the sum of squares within the strata, while SST represents the total sum of squares of RSEI in the study area. The variable i denotes the stratification of each influencing factor, where i takes values from 1 to k . Moreover, N and N_i refer to the sample sizes of the entire study area and each stratum i , respectively. Lastly, σ^2 and σ_i^2 denote the variances of the whole study area and each stratum i , respectively.

3.6. EE Trend Analysis

R/S analysis, also known as rescaled range analysis, is a statistical test applied to a time series [50]. The R/S analysis utilizes the least squares method, and the slope of the regression line equation represents the Hurst exponent (H). The Hurst exponent is linearly fitted using the least squares method, and relevant conclusions are drawn based on the results. The Hurst index can be used to analyze a set of time-series data, which change randomly with time. In this study, we utilize the Hurst index to monitor the variation of RSEI [51].

The basic principle of R/S analysis: For a time series $\{RSEI(\tau)\}, t = 1, 2, 3, \dots, \tau$, where τ is the total number of subseries in the time series $RSEI_t$.

Define the mean series:

$$\overline{RSEI}(\tau) = \frac{1}{\tau} \sum_{t=1}^{\tau} RSEI(t), (t = 1, 2, 3, \dots, \tau) \tag{19}$$

Cumulative deviation:

$$X(t, \tau) = \sum_{t=1}^{\tau} [RSEI(t) - \overline{RSEI}(\tau)], (1 \leq t \leq \tau) \tag{20}$$

Extreme deviation:

$$R(\tau) = \max_{1 \leq t \leq \tau} X(t, \tau) - \min_{1 \leq t \leq \tau} X(t, \tau), (t = 1, 2, 3, \dots, \tau) \tag{21}$$

Standard deviation:

$$S(\tau) = \left[\frac{1}{\tau} \sum_{t=1}^{\tau} (RSEI(t) - \overline{RSEI}(\tau))^2 \right]^{\frac{1}{2}}, (t = 1, 2, 3, \dots, \tau) \tag{22}$$

The Hurst index H is defined based on the asymptotic behavior of the rescaled extreme difference range as a function of the time span of the time series.

$$\log(R_t/S_t)_\tau = \log(C) + H \times \log(n), \tag{23}$$

where R_t/S_t denotes the rescaled extreme deviation range, C is a constant, n is the series length, and H is the Hurst index with a value domain of $[0, 1]$. In this study, we selected RSEI data from 2002–2022 for Hurst index analysis. When $H = 0.5$, the time series are completely independent; when $0 < H < 0.5$, the future change is opposite to the past, and the closer H is to 0.0, the stronger the inverse persistence; when $0.5 < H < 1.0$, the future change is consistent with the past change, and the closer H is to 1.0, the stronger the persistence.

3.7. Technical Pathway and Workflow

This paper comprises two parts. The first part involves the analysis of temporal variations in the EE in typical regions of CLP from 2002 to 2022, while the second part concerns the analysis of the spatial characteristics of the EE in these regions. To calculate NDVI, WET, NDBSI, and LST, MODIS data was utilized with the aid of GEE. After normalizing the four indicators to values between 0 and 1, the RSEI was computed using PCA. With RSEI serving as a measure of the EE, the study followed the analytical framework outlined below as Figure 3:

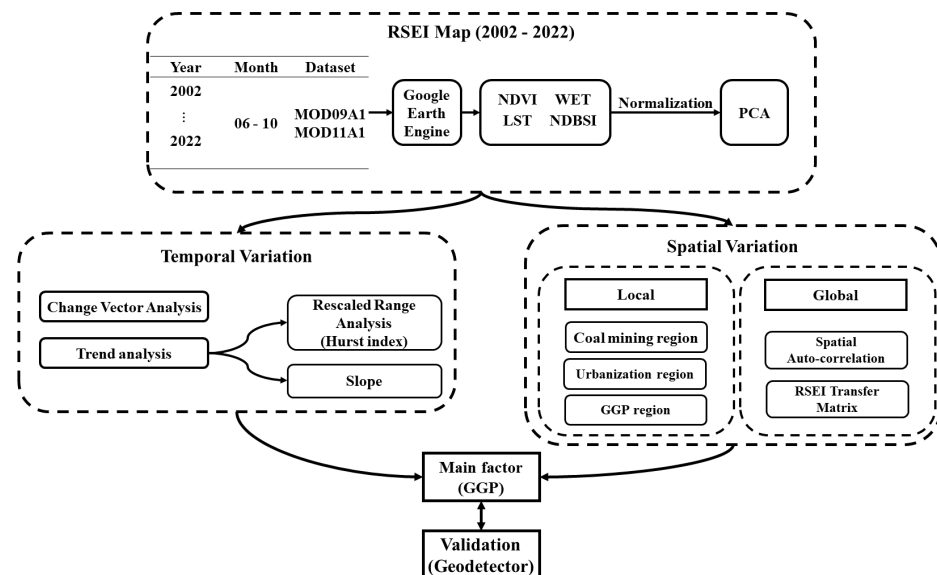


Figure 3. Analysis Framework of the RSEI in CLP.

1. On the temporal scale, the changes in EE in the study area since 2002 were evaluated. Specifically, the years 2002, 2007, 2012, 2017, and 2022 were chosen, and the EE was divided into five levels, with the area of each level counted. The change in EE between two years was obtained by CVA. Additionally, the trend analysis method was employed using the long RSEI time series results from 2002–2022 to obtain the slope index, and the Hurst index was used to analyze the trends in EE.
2. Three typical regions (the coal mining region, the urban region, and the GGP region) were chosen for the local spatial change analysis of the EE. The global spatial change

characteristics of the EE in the whole study area were analyzed by the Moran index, Lisa clustering, and transfer matrix. Geodetector was introduced to analyze and verify the study results.

4. Results

4.1. Temporal Variation of RSEI from 2002–2022

In the whole study area, we calculated the NDVI, WET, NDBSI, and LST using the GEE for the period of 2000–2022. Then, we applied PCA to obtain the RSEI, as shown in Figure 4.

The EE has been consistently improving since 2002, with the fitted curve showing logarithmic growth. The RSEI curve had a steep slope before 2007, but the rate of increase slowed down in the later period. To study this trend more closely, we selected the RSEI values from June to October of 2002, 2007, 2012, 2017, and 2022, which were 0.500, 0.542, 0.556, 0.558, and 0.577, respectively, as shown in Figure 5.

Over time, the RSEI has continued to increase, indicating an improvement in EE. The contribution of PC1 in the five images was 87.9%, 84.8%, 83.4%, 87.6%, and 85.4%, respectively, with a contribution over 80%. Among the four indicators of RSEI, NDVI and WET are positive impact indicators, while NDBSI and LST are negative impact indicators. The positive and negative indicators have opposite effects on the EE.

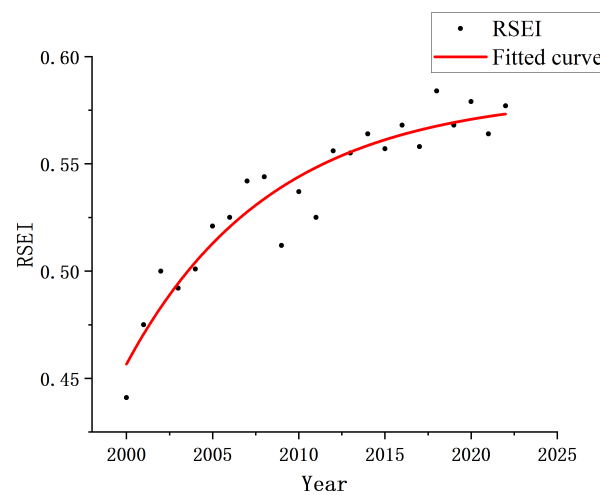


Figure 4. A logarithmic growth in EE improvement since 2002.

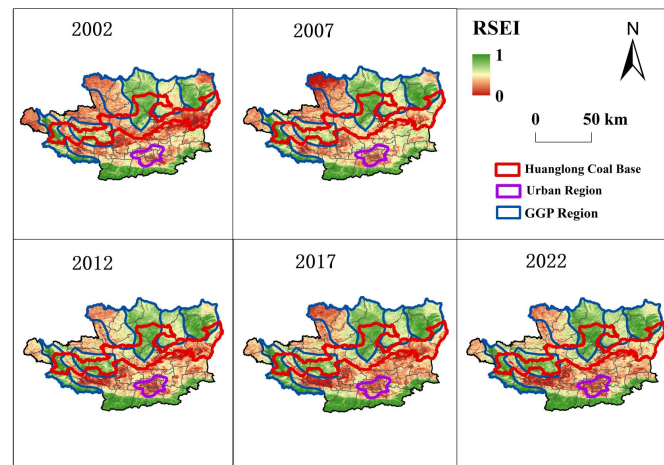


Figure 5. RSEI from June to October of 2002, 2007, 2012, 2017, and 2022.

To more clearly demonstrate how the EE has changed over time, the RSEI of the five years was divided into five levels: [0,0.2), [0.2,0.4), [0.4–0.6), [0.6–0.8), and [0.8–1.0), which are expressed as poor, fair, moderate, good, and excellent, respectively. The spatial distribution of the EE levels in these five years is shown in Figure 6.

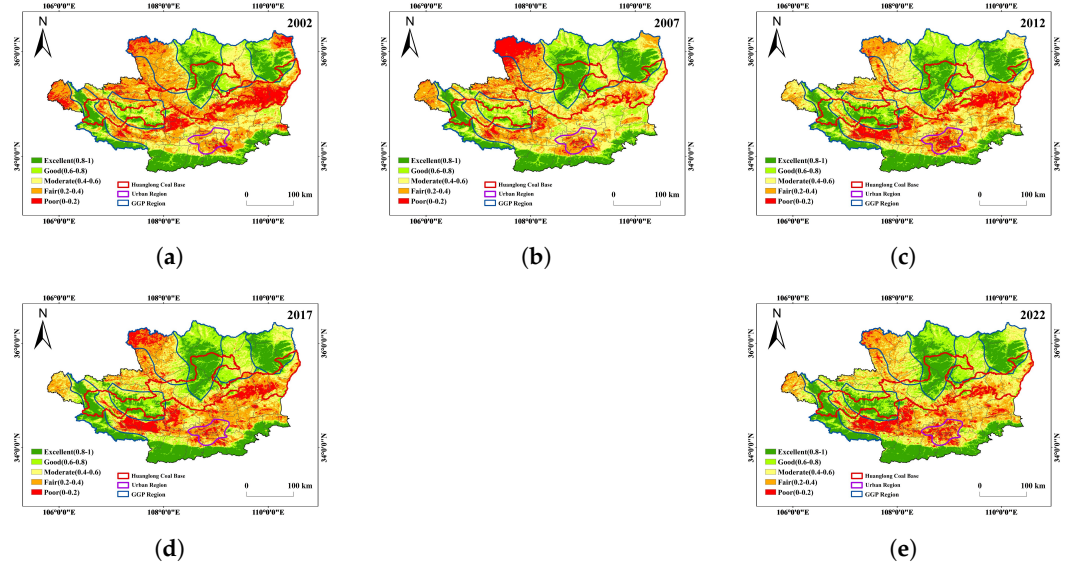


Figure 6. Spatial distribution of EE levels: (a) 2002, (b) 2007, (c) 2012, (d) 2017, and (e) 2022.

Compared to 2002, the EE mainly improved in the GGP region, while it became worse in the regions around the Guanzhong plain urban agglomeration and Huanglong coal base, and other local regions. In the GGP region, the percentages of poor and fair decreased significantly, while the percentages of good and excellent increased significantly. The percentages of moderate rose and then fell, indicating that some regions changed from poor to excellent.

On the other hand, the distribution characteristics of RSEI over time in different years were analyzed via CVA. The results are shown in Figure 7.

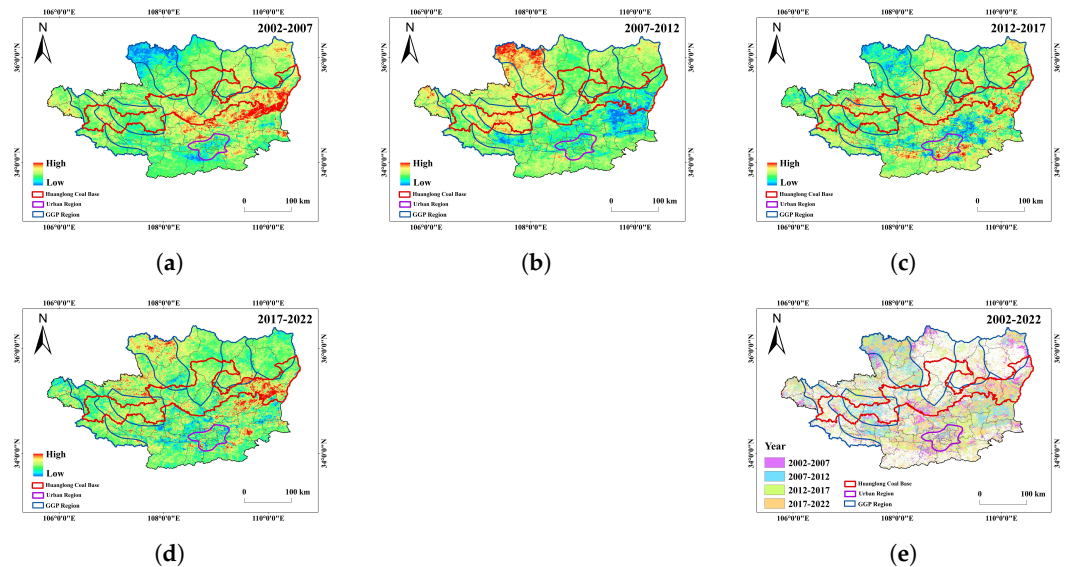


Figure 7. Variation magnitude map of the RSEI in the study area: (a) variation in 2002–2007, (b) variation in 2007–2012, (c) variation in 2012–2017, (d) variation in 2017–2022, and (e) variation intensity map of RSEI.

The high values of the amplitude of ecological changes $|\Delta V|$ are indicated in red, and the red areas are mostly continuously distributed from 2002 to 2007 and from 2007 to 2012,

and are more obvious in the Huanglong coal base and the northern GGP region. In 2012 to 2017 and 2017 to 2022, the red regions are mostly discretely distributed, more obvious in the east of the Huanglong coal base and urban regions.

4.2. Spatial Variation of the EE from 2002–2022

4.2.1. Local Spatial Variation in the EE in the Study Area

Although there has been an overall improvement in the EE since 2002, the local changes in the study area remain unclear [52]. To better understand the spatial characteristics of regional EE changes in different regions (that is, the coal mining region, the GGP region, and the urbanization region) under the influence of human projects, RSEI from 2002–2022 was analyzed. Figure 8 shows the variation in different land use types in 2002 and 2022. It is evident that the area of the GGP region (e.g., B1, B2, and B3) and the urbanization region (A) has significantly increased in the last 20 years, while the area of arable land has decreased. However, changes in land use types in the Huanglong coal base are difficult to distinguish directly. Further analysis on this area is presented below.

Taking the Dafosi coal mine in the Huanglong coal base as an example (as shown in Figure 9), we analyze the influence of coal mining activity on the local EE. The Dafosi coal mine is located in a loess hilly-gully region, with a mining area of about 70 km² and a total coal reserve of 765 Mt. Coal mining activity began in 2007, with a designed annual coal mining capacity of 8 million tons and a service life of 70 years [3,53]. The distribution of the annual mining workings of the Dafosi coal mine is shown in Figure 9.

After underground coal mining, a large-scale subsidence basin with a maximum subsidence value of more than 7 m will form on the ground. As shown in Figure 2, this will lead to serious damage to land resources and construction facilities and further cause environmental damage, such as soil erosion, lowering of the groundwater level, and vegetation withering [54]. The area of the coal mining region and surface subsidence region of the Dafosi coal mine from 2007 to 2022 is shown in Table 4 [55].

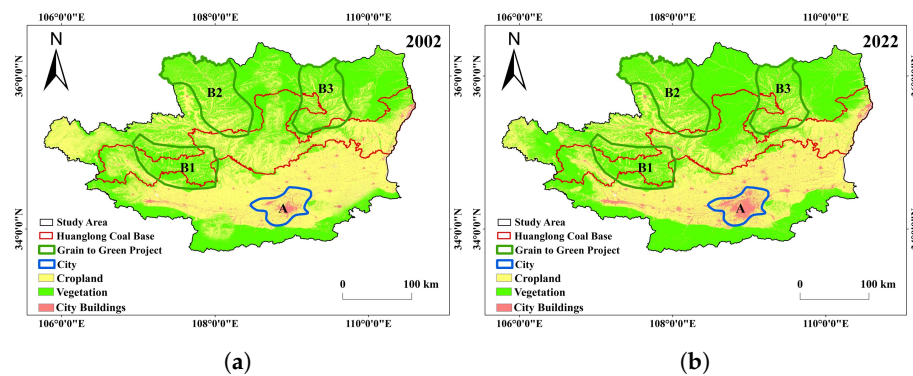


Figure 8. Land use type map in (a) 2002, and (b) 2022.

Table 4. The area of upper and lower coal mining from 2005 to 2022.

Year	Mining Area (km ²)	Subsidence Area (km ²)	Year	Mining Area (km ²)	Subsidence Area (km ²)
2007	0.343	0.785	2015	0.541	1.215
2008	0.490	1.220	2016	0.844	1.940
2009	0.451	1.137	2017	0.842	1.484
2010	0.558	1.290	2018	0.843	1.715
2011	0.592	1.172	2019	0.527	1.248
2012	0.672	1.455	2020	0.575	1.320
2013	0.828	2.050	2021	0.782	1.645
2014	0.777	2.125	2022	0.637	1.530

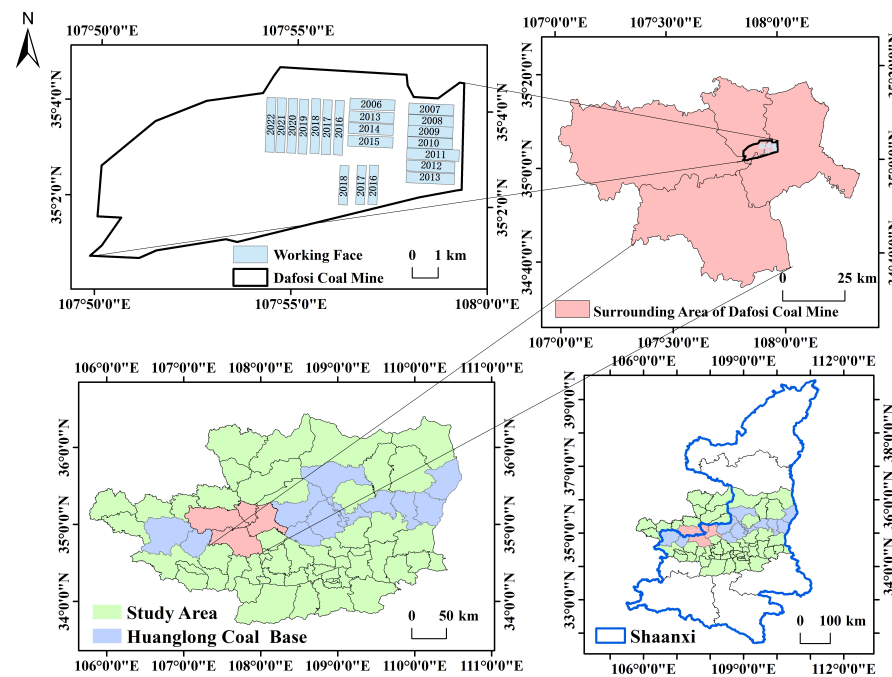


Figure 9. Location of Dafosi coal mine in China Loess Plateau (CLP) and Shaanxi province.

To quantitatively analyze the influence of subsidence on the surrounding EE in the Dafosi coal mine, the surface subsidence region was considered as the direct impact area of coal mining, and the indirect impact area (called the buffer area) was expanded by 3 km outward. The area to the east of the buffer area, which had not yet been affected by coal mining and had similar geographic conditions, was taken as the comparison area. The location of these three areas can be found in Figure 10. The RSEI values for the three areas were calculated from 2002–2022 and compared, as shown in Figure 11. Statistical analysis of the RSEI values of the three areas shows that the RSEI of the direct impact area of coal mining in the Dafosi mine has a high correlation with the RSEI of the buffer area and the comparison area, with correlation coefficients of 0.967 and 0.941, respectively. This means that the RSEI values of the direct impact area, buffer area, and comparison area are highly correlated, and the trend of all three is consistent, with an overall increasing trend. However, in the vast majority of years, the annual average RSEI in the direct impact area is smaller than that in the buffer area, while the annual average RSEI in the buffer area is smaller than that in the comparison area. After the Dafosi coal mine started mining in 2007, the annual average RSEI value in the direct impact area was 0.552, the annual average RSEI value in the buffer area was 0.576, and the annual average RSEI value in the comparison area was 0.596. The annual average RSEI value in the direct impact area was 4.1% lower than that in the buffer area and 7.3% lower than that in the comparison area. Further analysis shows that the difference between the RSEI values of the three areas was very small and remained almost equal during the period 2002–2006. This indicates that before coal mining began in 2007, the EE quality of the three regions was almost the same. After 2007, especially during 2009–2017, the EE quality of the direct impact area deteriorated significantly, indicating that underground coal mining had a significant negative impact on the surface EE in the mining area. The impact was mainly limited to the subsidence region, and the impact on the surrounding buffer area was relatively small.

In Figure 8, the urban region (A) and the typical GGP region (B1) were selected to analyze the EE variation of the above local region from 2002 to 2022, as shown in Figure 12.

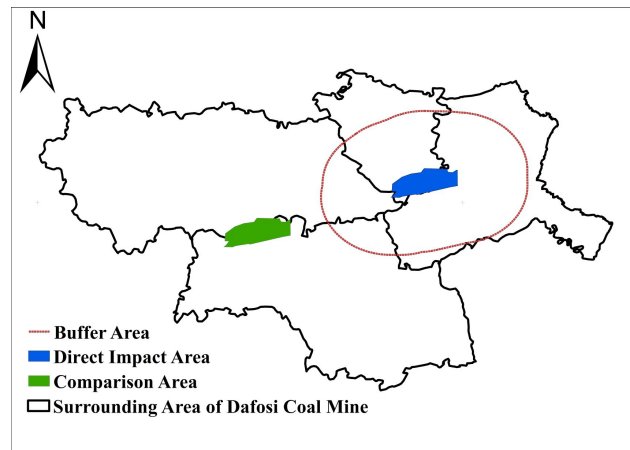


Figure 10. Locations of the coal mine area, buffer area, and comparison area.

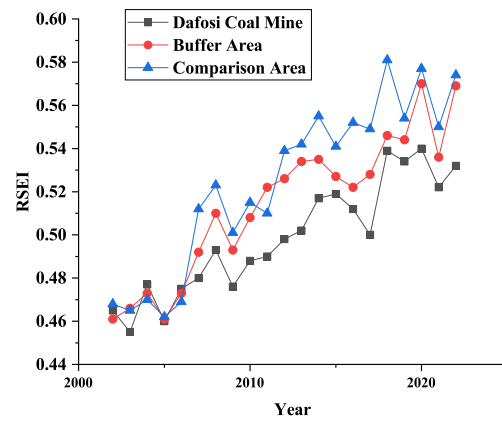


Figure 11. Changes in RSEI in coal mine area, buffer area, and comparison area from 2005 to 2022.

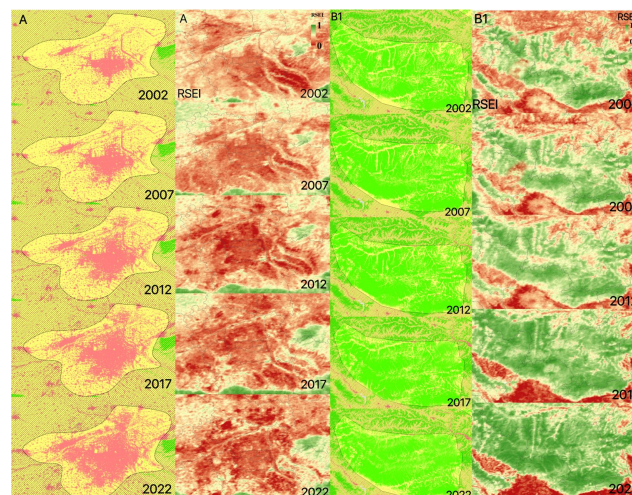


Figure 12. Local land use type and RSEI change in A (urban region) and B1 (part of GGP region) from 2002 to 2022.

From 2002 to 2022, the EE of the urban region continued to deteriorate as the area of Guanzhong plain urban agglomeration centered on Xi’an increased, and there was an obvious negative correlation between the two. Urbanization only affects the local EE and has a smaller impact on the EE of the entire study area because the area of the urban region makes up a small portion of the entire study area, similar to the mining region.

From 2002 to 2022, with GGP implemented, the area of forest and grassland continued to increase, and the EE in the typical GGP region (B1) became significantly better, and there was a high correlation between the two. The same is true for the other typical areas, B2 and B3 in Figure 8.

From the above analysis, it can be seen that two human projects, underground coal mining, and urbanization have significant negative impacts on the local EE, but the scope of such impact is relatively small and the impact on the ecological variation trend is relatively small. However, the GGP is the main factor driving the improvement in EE.

4.2.2. Global Spatial Variation of EE in the Study Area

To ensure the accuracy of the scale information, a $1 \text{ km} \times 1 \text{ km}$ grid was used to resample the RSEI images, and 83,745 sample points were collected in each RSEI image. The global Moran index and local LISA clustering were used to perform spatial autocorrelation analysis. The global Moran index determines whether there is spatial autocorrelation in the EE, while the local LISA index can obtain the spatial autocorrelation of the local EE. Figure 13 shows the global Moran index of the EE.

The global Moran index for 2002, 2007, 2012, 2017, and 2022 were 0.901, 0.923, 0.936, 0.937, and 0.966, respectively. These data indicate a very strong spatial correlation between the EE. Considering that the first and third quadrants contained the majority of the sample points, that is, H-H and L-L clustering, the study area indicates strong ecological aggregation characteristics. From 2002 to 2022, the Moran index showed a continuous upward trend, which was consistent with the changes in EE in the study area. Using local spatial autocorrelation, LISA clustering maps were created to show the exact distribution characteristics of the EE, as shown in Figure 14.

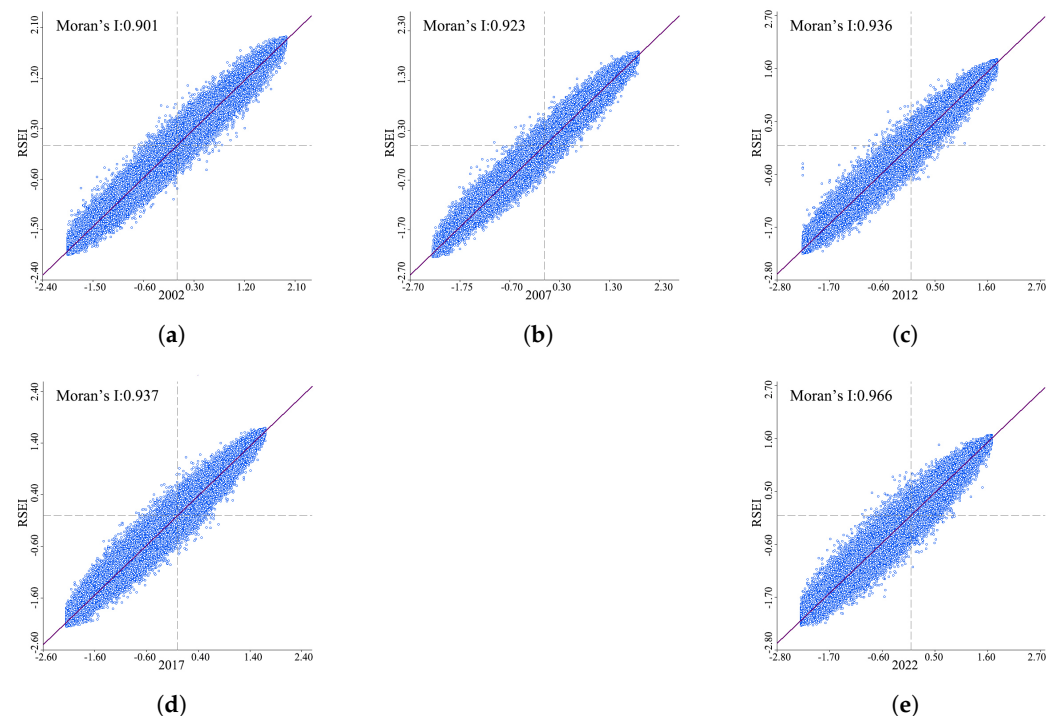


Figure 13. Global Moran index in the study area in (a) 2002, (b) 2007, (c) 2012, (d) 2017, and (e) 2022.

The LISA cluster distribution map shows that H-H is mainly distributed in the loess hilly-gully regions, and the vegetation cover in these areas has increased year by year due to the GGP policy. The distribution area of H-H increased rapidly between 2002 and 2012, until the vegetation entered the ecological succession stage in recent years, indicating that the GGP has improved the EE. On the other hand, L-L is mainly distributed in the river valley plain region, where urbanization is rapid and human production activities

are numerous, leading to continuous expansion of the L-L distribution area. Especially in the heavily populated urban areas, the L-L area gradually expanded from 2007 to 2022, indicating that rapid urbanization causes the deterioration of the EE.

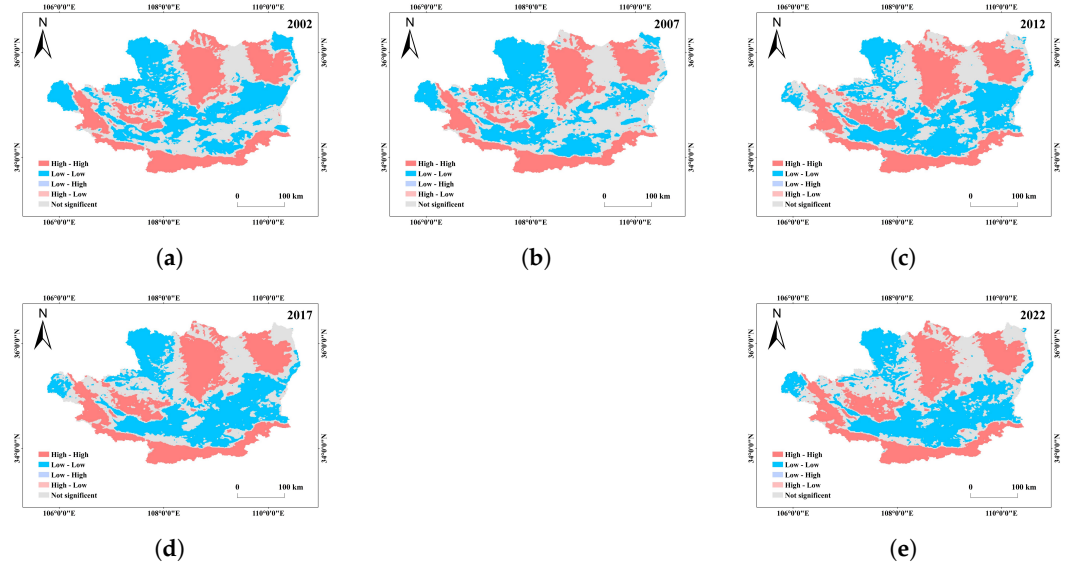


Figure 14. LISA clustering maps in the study area in (a) 2002, (b) 2007, (c) 2012, (d) 2017, and (e) 2022.

Furthermore, the chordal graph of RSEI transfer matrix is shown in Figure 15. Spatial transfer between different years is shown in the figure below, and the legend indicates the level of EE transfer (Figure 16). We also studied the transfer of EE since 2002.

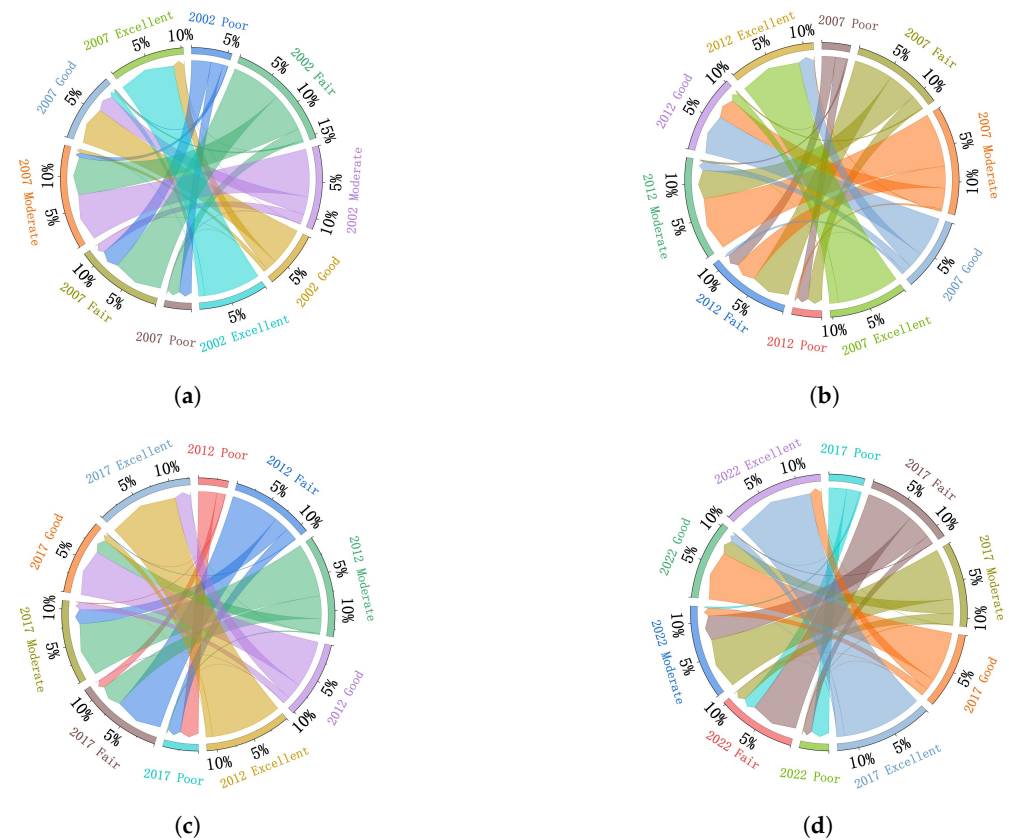


Figure 15. Chordal graph of RSEI transfer matrix of (a) 2002–2007, (b) 2007–2012, (c) 2012–2017, and (d) 2017–2022.

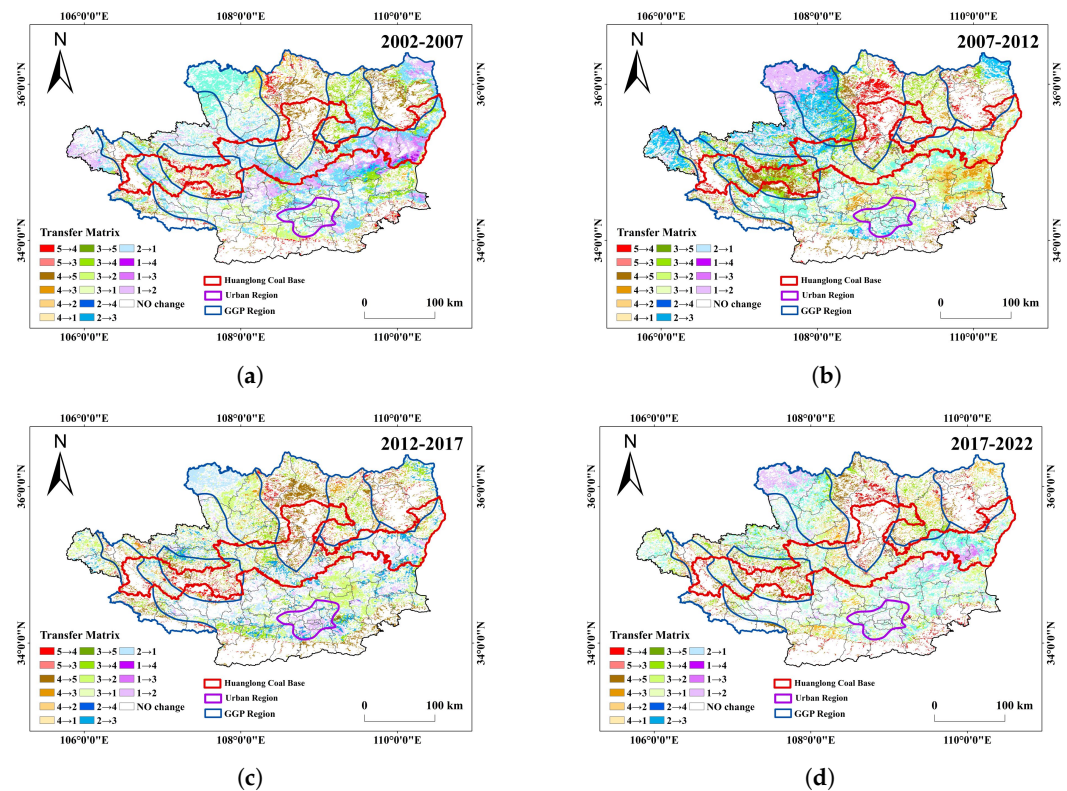


Figure 16. RSEI transfer matrix of (a) 2002–2007, (b) 2007–2012, (c) 2012–2017, and (d) 2017–2022.

The figure indicates that in many ecological improvement regions, Excellent areas increased to 21,777.36 km² by 2022. Except for a few regions that do not change, the transfer pattern is generally a poor, fair, and moderate transfer to each other; then a moderate, good, and excellent transfer to each other. In the period 2002–2007, a total area of 6124.77 km² was transferred from the poor regions, of which 4847.52 km² were transferred to the fair regions and 1178.36 km² were transferred to the moderate regions. In the period 2007–2012, a total area of 3572.21 km² was transferred from the poor regions, of which 3172.84 km² were transferred to the fair regions and 397 km² were transferred to the moderate regions. In the period 2012–2017, a total area of 2106 km² was transferred from the poor regions, of which 2007.76 km² were transferred to the fair regions and 97.24 km² were transferred to the moderate regions. In the period 2017–2022, a total area of 3485.81 km² was transferred from the poor regions, of which 3085.87 km² were transferred to the fair regions and 398.23 km² were transferred to the moderate regions.

Poor, fair, moderate, good, and excellent are defined as levels 1, 2, 3, 4, and 5, respectively. From 2002 to 2007, the EE in the study area changed considerably, with most of the regions changing within levels 2, 3, and 4. It should be noted that the EE of the GGP region changed to level 5 in a large area, while some parts of the mining region in the eastern section of the research area changed from level 1 to level 4. From 2007 to 2012, the EE changes were stable, and the EE in some parts of the GGP region was slightly degraded. From 2012 to 2017, the regions from level 4 to level 5 were scattered in the whole study area, and the EE slowly improved, and the environment in the river valley plain region improved. From 2017 to 2022, the area of the unchanged regions increased more than it did in the past and the EE is still slowly getting better. In general, the EE of the study area shows the results where it is rapidly getting better first, and then slowly getting better.

5. Discussion

5.1. Validation Based on Geodetector

In this study, it was concluded that the GGP has a major influence on the EE, while urbanization and coal mining have limited influence. It is known that meteorological

factors usually have a significant impact on the EE, with temperature and precipitation having a direct correlation with plant growth, and vegetation can promote EE improvement. To verify whether the GGP has the greatest driving force on the EE, we added temperature and precipitation as dependent variables, all five driving factors we selected can be found in Table 5 And the results are shown in Figure 17. The curves of RSEI and each driving factor with time are shown in Figure 18.

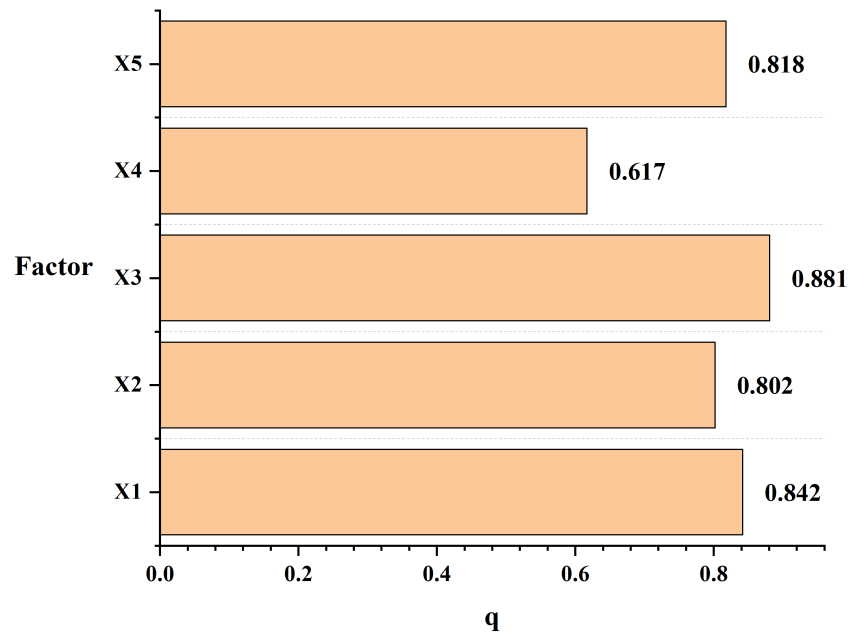


Figure 17. Q value of X1–X5.

Table 5. Driving factors.

Driving Factors	Factor Symbols	Unit	Type Numbers
Temperature	X1	°C	4
Precipitation	X2	mm	15
Grain for Green	X3	km ²	10
Raw coal	X4	Mt (Megatons)	15
GDP	X5	CNY/person	10

In the study area from June to October, X1 represents the average annual temperature, and X2 represents the average annual precipitation. The three types of human projects are represented by the X3 afforestation area, X4 annual coal production, and X5 GDP per capita, respectively. The results show that the factor with the greatest driving force on the EE is the Chinese government’s policy of GGP with a q value of 0.881, and the factor with the least driving force on the EE is the coal production in recent years with a q value of 0.617. Temperature and GDP per capita also significantly influence EE. Based on these findings, it can be concluded that GGP has the most significant impact on improving the EE of CLP.

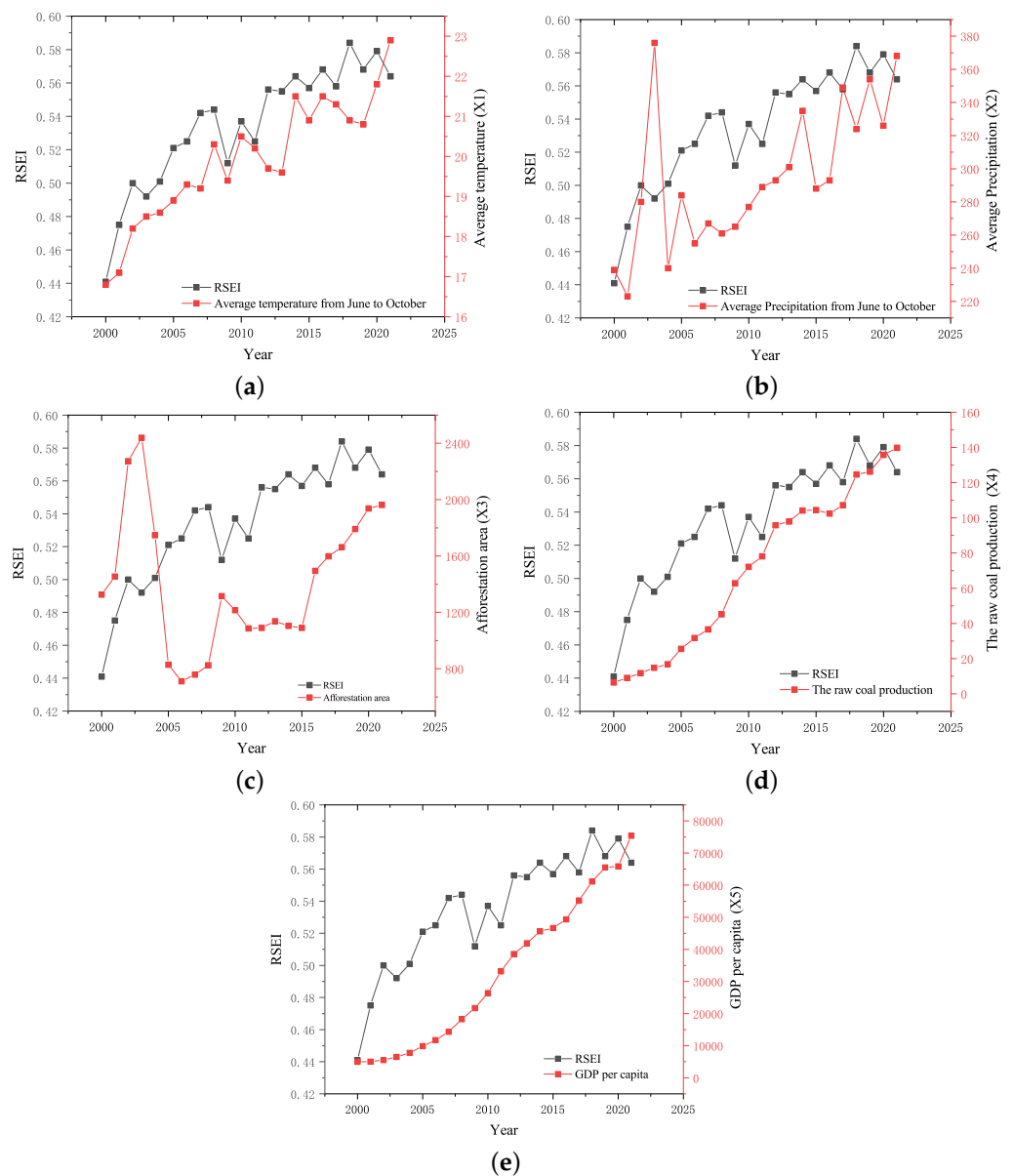


Figure 18. The RSEI and five driving factors (X1–X5) change curve. (a) RSEI and average annual temperature, (b) RSEI and average annual precipitation, (c) RSEI and afforestation area, (d) RSEI and raw coal, and (e) RSEI and GDP.

5.2. Trend Analysis of Ecological Changes in the Study Area

The trends of EE from 2002 to 2022 were analyzed statistically at the pixel scale. The geomorphological maps of the study area were then superimposed according to $Hurst > 0.5$ (indicating that the trend of EE is the same as in the past) and $Hurst < 0.5$ (indicating that the trend of EE is opposite to the past) after combining the slope index and significance test. This was performed to determine the spatial distribution of the Hurst index of different EE from 2002 to 2022, see Figure 19. To predict the EE trend, the slope index and Hurst index were combined, and the results are shown in Figure 20.

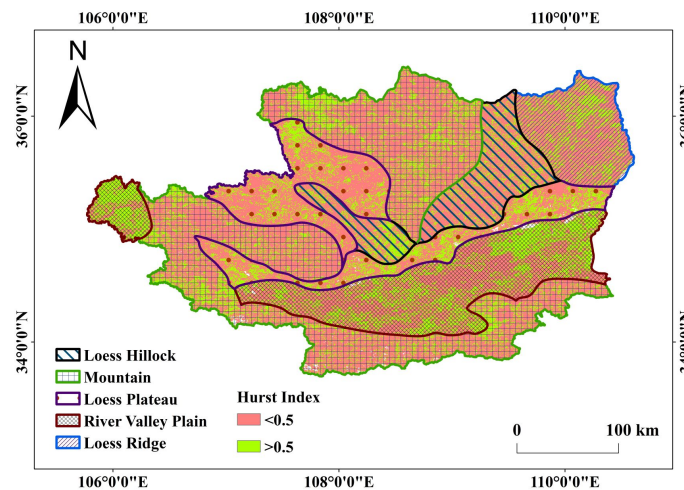


Figure 19. Hurst index map.

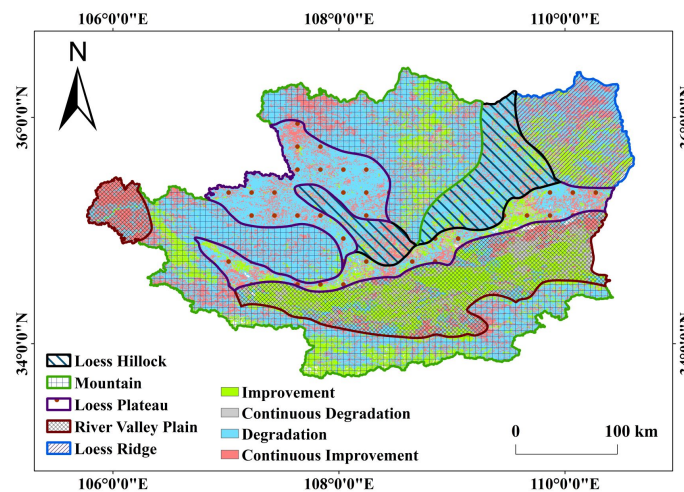


Figure 20. Future trend of EE.

According to the trend analysis graph, the majority of the area has a Hurst index of less than 0.5, indicating that most regions in the study area have an opposite trend of ecological change in the future compared to the past. The detail can be found in Table 6. The highest percentage of the region is moving from the state of past ecological improvement to the state of future ecological degradation, accounting for 51.94%. The area of regions with continuous improvement and the region from a past degradation state to possible future improvement state were 19% and 20.87%, respectively. From a geomorphological aspect, the EE of the river valley plain region still has potential for future improvement due to recent urbanization, while the vegetation cover of the loess hilly-gully region has already reached saturation and will enter the ecological succession stage in the future.

Table 6. Analysis of the trends obtained from long RSEI time series from 2002–2022.

Type of Change	Slope	Hurst	Area (km ²)	Pct.
Continuous degradation	<0	>0.5	6746.87	8.19
Degradation to improvement	<0	<0.5	15,648.18	19.00
Continuous improvement	>0	<0.5	17,193.62	20.87
improvement to Degradation	>0	>0.5	42,776.54	51.94

5.3. Comprehensive Analysis and Research Limitation

The spatial variation of EE quality in the typical CLP region generally agrees with the NDVI and WET indicators. The initial implementation of the GGP from 1999 to 2005 led to changes in vegetation types, but did not provide sufficient ecological benefits for soil water retention. However, due to the lagging effect of the GGP, vegetation cover in the typical CLP region increased and the EE quality significantly improved by around 2010.

Large-scale underground coal mining activities take place every year in the Huanglong coal base, causing significant subsidence on the surface. The groundwater level in the mining region and surrounding buffer zone has dropped significantly, and soil nutrients have been lost, resulting in the destruction of the levelness and water storage functions of arable land, causing farmers to abandon farming and impairing vegetation growth or causing it to die. According to statistics, the subsidence regions in the Huanglong coal base are not continuously distributed, and the area of subsidence regions formed by mining in each mine each year generally does not exceed 5 km². Therefore, the impact of coal mining activities on the EE is small in area and spatially discontinuous. It should be noted that with the Chinese government's increasingly stringent requirements for environmental protection in mining areas, coal mining enterprises have begun to carry out land remediation and ecological restoration in subsidence regions since 2015. Additionally, the recovery effect of rising temperatures and increased rainfall on the EE of subsidence regions has helped to mitigate the damage caused by coal mining activities, so the scope of the EE damage caused by coal mining activities is relatively small.

Since 2000, the Chinese government has proposed the China Western Development initiative, which has increased support for the Guanzhong district. The excessive economic development and population growth coincided with an increase in construction areas, leading to the occupation of nearby arable land and the expansion of industrial activities, increasing environmental pressures. The urbanization process has accelerated due to the creation of economic and high-tech zones, and the rapid growth of GDP per capita reflects the significant development achieved in the last two decades. The river valley plain area, with Xi'an as its central city, has experienced significant ecological degradation due to rapid urbanization, becoming the economic development center in western China. As a result, construction land and roads have expanded into grasslands and arable land. In 2012, the government proposed a strategy to promote ecological civilization, placing increasing emphasis on developing eco-cities [56]. The number of green belts and urban parks within the city has increased, contributing to the removal of urbanization's harmful effects on the local ecology [57].

Regarding landform, the EE of the loess hilly-gully region in the Loess Plateau mining area improved the most. Although coal mining has an impact on the nearby region, the GGP greatly improved the EE of the loess hilly-gully region, which entered the ecological succession stage at around 2020. Conversely, urban development led to EE deterioration in the river valley plain region, but thanks to the local government's urban environmental protection policies, published roughly in 2020, the EE of the river valley plain region has gradually improved and will continue to do so in the future.

It should be noted that this study mainly used RSEI to evaluate the EE quality in the typical region of CLP, which still has some limitations in terms of evaluation indices and data reliability. The study utilized MODIS remote sensing data with a spatial resolution of 500 m, and higher resolution remote sensing images will be utilized for future studies. Additionally, for EE prediction, the trend prediction will be changed to predicting the time period in the future to make the prediction more accurate.

6. Conclusions

In this paper, RSEI was used as an effective indicator for EE evaluation, and RSEI was calculated on the GEE. Using different methods, the variation of the EE since 2002 was analyzed comprehensively for the first time on temporal-spatial scales, and the EE impacts caused by three major human projects, GGP, coal mining activity, and urbanization, were

evaluated quantitatively. The effectiveness of the GGP policy was verified, and on this basis, the future trend of the CLP typical region was also predicted. The following is a summary of the key findings of this study:

1. Between 2002–2022, the EE of the study area has been improving under the policy of GGP, and the RSEI value has changed from 0.50 in 2002 to 0.577 in 2022, with a PC1 contribution rate of more than 83%. The results of this study agree with the data published by the Chinese government, and the applicability of the RSEI model to the study of the EE of CLP is validated.
2. The GGP implemented since 2000 is the key factor of the EE improvement in the study area. The GGP has achieved significant results, and there is no need to significantly increase the artificial vegetation. In this study, we validated that the GGP had the biggest influence on the EE of the study area using Geodetector [58,59].
3. The EE of the coal mining subsidence region in the Huanglong coal base deteriorated, but the negative impact of coal mining activities on the EE was small in scope and discrete in distribution; the China Western Development implemented by the Chinese government since 2000 has led to the rapid development of Guanzhong plain urban agglomeration, which significantly deteriorated the EE in and around the urban region, but the impact is also small in scope. Based on a series of environmental protection policies in recent years, the EE of the urban region is gradually improving.
4. Obvious temporal–spatial EE variation could be seen in CLP typical regions. The EE in the loess hilly-gully region changed from rapid improvement in the early phases to slow improvement in the later phases, and was predicted to enter the ecological succession stage in the future; the EE in the river valley plain regions changed from rapid deterioration in the early phases to slow improvement in the later phases, and was predicted to tend to improve gradually in the future.

This study provides a strong scientific basis for evaluating EE protection and the sustainable development of CLP.

Author Contributions: Conceptualization, J.T.; methodology, J.T., L.S., Y.D., Q.Y., R.Z. and X.Q.; validation, J.T.; data curation, J.T.; writing—original draft preparation, J.T.; writing—review and editing, J.T. and L.S.; supervision, L.S.; funding acquisition, T.M. All authors have read and agreed to the published version of the manuscript.

Funding: This research was funded by the National Natural Science Foundation of China, grant number: 52274168.

Institutional Review Board Statement: Not applicable.

Informed Consent Statement: Not applicable.

Data Availability Statement: Not applicable.

Conflicts of Interest: The authors declare no conflict of interest.

References

1. Shi, H.; Shao, M. Soil and water loss from the Loess Plateau in China. *J. Arid. Environ.* **2000**, *45*, 9–20. [[CrossRef](#)]
2. Chen, G.; Zhang, Y.; Zeng, R.; Yang, Z.; Chen, X.; Zhao, F.; Meng, X. Detection of land subsidence associated with land creation and rapid urbanization in the Chinese loess plateau using time series insar: A case study of Lanzhou new district. *Remote Sens.* **2018**, *10*, 270. [[CrossRef](#)]
3. Tang, J.; Sui, L. Geodetector-Based Livability Analysis of Potential Resettlement Locations for Villages in Coal Mining Areas on the Loess Plateau of China. *Sustainability* **2022**, *14*, 8365. [[CrossRef](#)]
4. Wang, L.; Shao, M.; Wang, Q.; Gale, W.J. Historical changes in the environment of the Chinese Loess Plateau. *Environ. Sci. Policy* **2006**, *9*, 675–684. [[CrossRef](#)]
5. Lai, H.H. China's western development program: Its rationale, implementation, and prospects. *Mod. China* **2002**, *28*, 432–466. [[CrossRef](#)]
6. Zhuo, C.; Deng, F. How does China's Western Development Strategy affect regional green economic efficiency? *Sci. Total. Environ.* **2020**, *707*, 135939. [[CrossRef](#)]

7. Uchida, E.; Xu, J.; Rozelle, S. Grain for green: Cost-effectiveness and sustainability of China's conservation set-aside program. *Land Econ.* **2005**, *81*, 247–264. [[CrossRef](#)]
8. Feng, Z.; Yang, Y.; Zhang, Y.; Zhang, P.; Li, Y. Grain-for-green policy and its impacts on grain supply in West China. *Land Use Policy* **2005**, *22*, 301–312. [[CrossRef](#)]
9. Wu, X.; Wang, S.; Fu, B.; Feng, X.; Chen, Y. Socio-ecological changes on the Loess Plateau of China after Grain to Green Program. *Sci. Total. Environ.* **2019**, *678*, 565–573. [[CrossRef](#)]
10. Tsunekawa, A.; Liu, G.; Yamanaka, N.; Du, S. *Restoration and Development of the Degraded Loess Plateau, China*; Springer: Berlin/Heidelberg, Germany, 2014. [[CrossRef](#)]
11. Guobin, L. Soil conservation and sustainable agriculture on the Loess Plateau: Challenges and prospects. *Ambio* **1999**, *28*, 663–668.
12. Hu, S.; Zhi-mao, G.; Jun-ping, Y. The impacts of urbanization on soil erosion in the Loess Plateau region. *J. Geogr. Sci.* **2001**, *11*, 282–290. [[CrossRef](#)]
13. Xu, D.; Yang, F.; Yu, L.; Zhou, Y.; Li, H.; Ma, J.; Huang, J.; Wei, J.; Xu, Y.; Zhang, C.; et al. Quantization of the coupling mechanism between eco-environmental quality and urbanization from multisource remote sensing data. *J. Clean. Prod.* **2021**, *321*, 128948. [[CrossRef](#)]
14. Han, T.; Lu, H.; Lü, Y.; Fu, B. Assessing the effects of vegetation cover changes on resource utilization and conservation from a systematic analysis aspect. *J. Clean. Prod.* **2021**, *293*, 126102. [[CrossRef](#)]
15. Xie, X.; Xu, C.; Wen, Y.; Li, W. Monitoring groundwater storage changes in the Loess Plateau using GRACE satellite gravity data, hydrological models and coal mining data. *Remote Sens.* **2018**, *10*, 605. [[CrossRef](#)]
16. Unlu, T.; Akcin, H.; Yilmaz, O. An integrated approach for the prediction of subsidence for coal mining basins. *Eng. Geol.* **2013**, *166*, 186–203. [[CrossRef](#)]
17. Bradley, C.A.; Altizer, S. Urbanization and the ecology of wildlife diseases. *Trends Ecol. Evol.* **2007**, *22*, 95–102. [[CrossRef](#)]
18. Wang, J.; Wang, Z.; Cheng, H.; Kang, J.; Liu, X. Land Cover Changing Pattern in Pre-and Post-Earthquake Affected Area from Remote Sensing Data: A Case of Lushan County, Sichuan Province. *Land* **2022**, *11*, 1205. [[CrossRef](#)]
19. Yurui, L.; Xuanchang, Z.; Zhi, C.; Zhengjia, L.; Zhi, L.; Yansui, L. Towards the progress of ecological restoration and economic development in China's Loess Plateau and strategy for more sustainable development. *Sci. Total. Environ.* **2021**, *756*, 143676. [[CrossRef](#)]
20. Chen, W.; Xu, Q.; Zhao, K.; Zhou, X.; Li, S.; Wang, J.; Wang, X.; Xu, J. Spatial analysis of land-use management for gully land consolidation on the Loess Plateau in China. *Ecol. Indic.* **2020**, *117*, 106633. [[CrossRef](#)]
21. Xu, H.; Wang, M.; Shi, T.; Guan, H.; Fang, C.; Lin, Z. Prediction of ecological effects of potential population and impervious surface increases using a remote sensing based ecological index (RSEI). *Ecol. Indic.* **2018**, *93*, 730–740. [[CrossRef](#)]
22. Xu, H.; Wang, Y.; Guan, H.; Shi, T.; Hu, X. Detecting ecological changes with a remote sensing based ecological index (RSEI) produced time series and change vector analysis. *Remote Sens.* **2019**, *11*, 2345. [[CrossRef](#)]
23. Liao, W. Temporal and spatial variations of eco-environment in Association of Southeast Asian Nations from 2000 to 2021 based on information granulation. *J. Clean. Prod.* **2022**, *373*, 133890. [[CrossRef](#)]
24. Yuan, B.; Fu, L.; Zou, Y.; Zhang, S.; Chen, X.; Li, F.; Deng, Z.; Xie, Y. Spatiotemporal change detection of ecological quality and the associated affecting factors in Dongting Lake Basin, based on RSEI. *J. Clean. Prod.* **2021**, *302*, 126995. [[CrossRef](#)]
25. Kang, J.; Wang, Z.; Cheng, H.; Wang, J.; Liu, X. Remote Sensing Land Use Evolution in Earthquake-Stricken Regions of Wenchuan County, China. *Sustainability* **2022**, *14*, 9721. [[CrossRef](#)]
26. Ning, T.; Liu, W.; Lin, W.; Song, X. NDVI variation and its responses to climate change on the northern Loess Plateau of China from 1998 to 2012. *Adv. Meteorol.* **2015**, *2015*, 725427. [[CrossRef](#)]
27. Xiao, J. Satellite evidence for significant biophysical consequences of the “Grain for Green” Program on the Loess Plateau in China. *J. Geophys. Res. Biogeosci.* **2014**, *119*, 2261–2275. [[CrossRef](#)]
28. Lu, H.; Liu, W.; Yang, H.; Wang, H.; Liu, Z.; Leng, Q.; Sun, Y.; Zhou, W.; An, Z. 800-kyr land temperature variations modulated by vegetation changes on Chinese Loess Plateau. *Nat. Commun.* **2019**, *10*, 1958. [[CrossRef](#)]
29. Abdi, H.; Williams, L.J. Principal component analysis. *Wiley Interdiscip. Rev. Comput. Stat.* **2010**, *2*, 433–459. [[CrossRef](#)]
30. Shan, W.; Jin, X.; Ren, J.; Wang, Y.; Xu, Z.; Fan, Y.; Gu, Z.; Hong, C.; Lin, J.; Zhou, Y. Ecological environment quality assessment based on remote sensing data for land consolidation. *J. Clean. Prod.* **2019**, *239*, 118126. [[CrossRef](#)]
31. Wen, X.; Ming, Y.; Gao, Y.; Hu, X. Dynamic monitoring and analysis of ecological quality of pingtan comprehensive experimental zone, a new type of sea island city, based on RSEI. *Sustainability* **2019**, *12*, 21. [[CrossRef](#)]
32. Ning, L.; Jiayao, W.; Fen, Q. The improvement of ecological environment index model RSEI. *Arab. J. Geosci.* **2020**, *13*, 1–14. [[CrossRef](#)]
33. Wang, J.; Yang, X.; Wang, Z.; Cheng, H.; Kang, J.; Tang, H.; Li, Y.; Bian, Z.; Bai, Z. Consistency Analysis and Accuracy Assessment of Three Global Ten-Meter Land Cover Products in Rocky Desertification Region—A Case Study of Southwest China. *ISPRS Int. J. Geo-Inf.* **2022**, *11*, 202. [[CrossRef](#)]
34. Gorelick, N.; Hancher, M.; Dixon, M.; Ilyushchenko, S.; Thau, D.; Moore, R. Google Earth Engine: Planetary-scale geospatial analysis for everyone. *Remote Sens. Environ.* **2017**, *202*, 18–27. [[CrossRef](#)]
35. Huang, H.; Chen, W.; Zhang, Y.; Qiao, L.; Du, Y. Analysis of ecological quality in Lhasa Metropolitan Area during 1990–2017 based on remote sensing and Google Earth Engine platform. *J. Geogr. Sci.* **2021**, *31*, 265–280. [[CrossRef](#)]

36. Hou, H.; Ding, Z.; Zhang, S.; Guo, S.; Yang, Y.; Chen, Z.; Mi, J.; Wang, X. Spatial estimate of ecological and environmental damage in an underground coal mining area on the Loess Plateau: Implications for planning restoration interventions. *J. Clean. Prod.* **2021**, *287*, 125061. [[CrossRef](#)]
37. Zhou, D.; Zhao, S.; Zhu, C. The Grain for Green Project induced land cover change in the Loess Plateau: A case study with Ansai County, Shanxi Province, China. *Ecol. Indic.* **2012**, *23*, 88–94. [[CrossRef](#)]
38. Kang, J.; Yang, X.; Wang, Z.; Cheng, H.; Wang, J.; Tang, H.; Li, Y.; Bian, Z.; Bai, Z. Comparison of Three Ten Meter Land Cover Products in a Drought Region: A Case Study in Northwestern China. *Land* **2022**, *11*, 427. [[CrossRef](#)]
39. Xiang, K.; Zhao, A.; Liu, H.; Zhang, X.; Zhang, A.; Tian, X.; Jin, Z. Spatiotemporal Evolution and Coupling Pattern Analysis of Urbanization and Ecological Environmental Quality of the Chinese Loess Plateau. *Sustainability* **2022**, *14*, 7236. [[CrossRef](#)]
40. Wang, Y.; Fu, B.; Chen, L.; Lu, Y.; Gao, Y. Check dam in the Loess Plateau of China: Engineering for environmental services and food security. *Environ. Sci. Technol.* **2011**, *45*, 10298–10299. [[CrossRef](#)]
41. Chen, N.; Ma, T.; Zhang, X. Responses of soil erosion processes to land cover changes in the Loess Plateau of China: A case study on the Beiluo River basin. *Catena* **2016**, *136*, 118–127. [[CrossRef](#)]
42. Cao, S.; Chen, L.; Yu, X. Impact of China's Grain for Green Project on the landscape of vulnerable arid and semi-arid agricultural regions: A case study in northern Shaanxi Province. *J. Appl. Ecol.* **2009**, *46*, 536–543. [[CrossRef](#)]
43. Shang, Y.; Lu, S.; Li, X.; Hei, P.; Lei, X.; Gong, J.; Liu, J.; Zhai, J.; Wang, H. Balancing development of major coal bases with available water resources in China through 2020. *Appl. Energy* **2017**, *194*, 735–750. [[CrossRef](#)]
44. Zhao, C.; Duan, D.; Li, Y.; Zhang, J. Rare earth elements in No. 2 coal of Huangling mine, Huanglong coalfield, China. *Energy Explor. Exploit.* **2012**, *30*, 803–818. [[CrossRef](#)]
45. Baig, M.H.A.; Zhang, L.; Shuai, T.; Tong, Q. Derivation of a tasselled cap transformation based on Landsat 8 at-satellite reflectance. *Remote Sens. Lett.* **2014**, *5*, 423–431. [[CrossRef](#)]
46. Chen, Y. New approaches for calculating Moran's index of spatial autocorrelation. *PLoS ONE* **2013**, *8*, e68336. [[CrossRef](#)]
47. Boori, M.S.; Choudhary, K.; Paringer, R.; Kupriyanov, A. Spatiotemporal ecological vulnerability analysis with statistical correlation based on satellite remote sensing in Samara, Russia. *J. Environ. Manag.* **2021**, *285*, 112138. [[CrossRef](#)]
48. Nie, X.; Hu, Z.; Zhu, Q.; Ruan, M. Research on temporal and spatial resolution and the driving forces of ecological environment quality in coal mining areas considering topographic correction. *Remote Sens.* **2021**, *13*, 2815. [[CrossRef](#)]
49. Gao, W.; Zhang, S.; Rao, X.; Lin, X.; Li, R. Landsat TM/OLI-Based Ecological and Environmental Quality Survey of Yellow River Basin, Inner Mongolia Section. *Remote Sens.* **2021**, *13*, 4477. [[CrossRef](#)]
50. Mandelbrot, B. Statistical methodology for nonperiodic cycles: From the covariance to R/S analysis. In *Annals of Economic and Social Measurement, Volume 1, Number 3*; NBER: Cambridge, MA, USA, 1972; pp. 259–290.
51. Wu, S.; Gao, X.; Lei, J.; Zhou, N.; Guo, Z.; Shang, B. Ecological environment quality evaluation of the Sahel region in Africa based on remote sensing ecological index. *J. Arid. Land* **2022**, *14*, 14–33. [[CrossRef](#)]
52. Wang, X.; Wu, J.; Liu, Y.; Hai, X.; Shangguan, Z.; Deng, L. Driving factors of ecosystem services and their spatiotemporal change assessment based on land use types in the Loess Plateau. *J. Environ. Manag.* **2022**, *311*, 114835. [[CrossRef](#)]
53. Sui, L.; Ma, F.; Chen, N. Mining subsidence prediction by combining support vector machine regression and interferometric synthetic aperture radar data. *ISPRS Int. J. Geo-Inf.* **2020**, *9*, 390. [[CrossRef](#)]
54. Kratzsch, H. *Mining Subsidence Engineering*; Springer Science & Business Media: Berlin/Heidelberg, Germany, 2012. [[CrossRef](#)]
55. Ma, S.; Qiu, H.; Yang, D.; Wang, J.; Zhu, Y.; Tang, B.; Sun, K.; Cao, M. Surface multi-hazard effect of underground coal mining. *Landslides* **2022**, *20*, 39–52. [[CrossRef](#)]
56. de Jong, M.; Yu, C.; Joss, S.; Wennersten, R.; Yu, L.; Zhang, X.; Ma, X. Eco city development in China: Addressing the policy implementation challenge. *J. Clean. Prod.* **2016**, *134*, 31–41. [[CrossRef](#)]
57. Dang, H.; Li, J.; Zhang, Y.; Zhou, Z. Evaluation of the equity and regional management of some urban green space ecosystem services: A case study of main urban area of Xi'an City. *Forests* **2021**, *12*, 813. [[CrossRef](#)]
58. Wang, J.F.; Li, X.H.; Christakos, G.; Liao, Y.L.; Zhang, T.; Gu, X.; Zheng, X.Y. Geographical detectors-based health risk assessment and its application in the neural tube defects study of the Heshun Region, China. *Int. J. Geogr. Inf. Sci.* **2010**, *24*, 107–127. [[CrossRef](#)]
59. Wang, J.F.; Zhang, T.L.; Fu, B.J. A measure of spatial stratified heterogeneity. *Ecol. Indic.* **2016**, *67*, 250–256. [[CrossRef](#)]

Disclaimer/Publisher's Note: The statements, opinions and data contained in all publications are solely those of the individual author(s) and contributor(s) and not of MDPI and/or the editor(s). MDPI and/or the editor(s) disclaim responsibility for any injury to people or property resulting from any ideas, methods, instructions or products referred to in the content.